

Article

Electromagnetic Field Analysis of Signal Transmission Path and Electrode Contact Conditions in Human Body Communication

Kentaro Yamamoto ^{1,*}, Yoshifumi Nishida ¹, Ken Sasaki ¹, Dairoku Muramatsu ² and Fukuro Koshiji ³

¹ Department of Human and Engineered Environmental Studies, Graduate School of Frontier Sciences, The University of Tokyo, 5-1-5 Kashiwanoha, Kashiwa-shi, Chiba-ken 277-8563, Japan; nishida@ems.k.u-tokyo.ac.jp (Y.N.); ksasaki@edu.k.u-tokyo.ac.jp (K.S.)

² Department of Electrical Engineering, Faculty of Science and Technology, Tokyo University of Science, 2641 Yamazaki, Noda-shi, Chiba-ken 278-8510, Japan; muramatsu@rs.tus.ac.jp

³ General Education and Research Center, Tokyo Polytechnic University, 1583 Iiyama, Atsugi-shi, Kanagawa-ken 243-0297, Japan; koshiji@gen.t-kougei.ac.jp

* Correspondence: kyamamoto@s.h.k.u-tokyo.ac.jp

Received: 12 July 2018; Accepted: 31 August 2018; Published: 3 September 2018



Abstract: Human body communication (HBC) is a wireless communication method that uses the human body as part of the transmission medium. Electrodes are used instead of antennas, and the signal is transmitted by the electric current through the human body and by the capacitive coupling outside the human body. In this study, direction of electric field lines and direction of electric current through the human body were analyzed by the finite-difference time-domain method to clarify the signal path, which is not readily apparent from electric field strength distribution. Signal transmission from a transmitter on the subject's wrist to an off-body receiver touched by the subject was analyzed for two types of transmitter electrode settings. When both the signal and ground electrodes were put in contact with the human body, the major return path consisted of capacitive coupling between the receiver ground and the human body, and the electric current through the human body that flowed back to the ground electrode of the transmitter. When the ground electrode was floating, the only return path was through the capacitive coupling of the floating ground. These results contribute to the better understanding of signal transmission mechanism of HBC and will be useful for developing HBC applications.

Keywords: human body communication; wireless body area networks; electromagnetic field analysis; capacitive coupling; electric-field distribution; finite-difference time-domain

1. Introduction

Human body communication (HBC) is a wireless communication method that uses the human body as part of the signal transmission medium, and it is expected to be among the technologies used in wireless body area networks [1]. In the IEEE (Institute of Electrical and Electronics Engineers) 802.15.6 standard, HBC was adopted as one of the three physical layers for the body area network. The other two layers are narrowband and ultra-wide band [2]. In comparison with other wireless communication technologies such as Bluetooth and Zigbee, HBC is advantageous in terms of its communication secrecy, low power consumption, and intuitive tactile operation. Because of these advantages, HBC is expected to be utilized in wearable devices for health care systems [3]. There are two transmission mechanisms of HBC: galvanic and capacitive coupling [4]. In galvanic HBC, the signal frequency is between 100 kHz and 10 MHz and the current flowing through the human body between the

transmitter and the receiver contributes to the transmission [5,6]. In capacitive coupling, the signal frequency is between 100 kHz and 100 MHz and the current through the human body and the electric field around the human body contribute to the transmission [7–10]. Detailed studies on the electric field distribution and its contribution to capacitive coupling have been carried out using calculation methods such as the finite element method (FEM) and the finite-difference time-domain method (FDTD) [11,12].

Although the conditions of the contact between the electrodes and the human body greatly influence the transmission characteristic of HBC, the electrode contact condition has not yet been standardized. The shape of HBC devices, and the electrode dimensions and arrangements, vary from study to study. In most HBC studies, researchers have adopted a one-electrode contact for both the transmitter and the receiver; the signal electrode is in contact with the human body while the ground electrode is left floating [13,14]. In recent years, some studies have used a two-electrode transmitter in which the signal and ground electrodes of the transmitter are both in contact with the human body. Some studies have compared the transmission characteristics and electric field distributions of one- and two-electrode contact transmitters [15–20]. Haga et al. conducted numerical simulation and investigated the difference between the received voltages and electric field distributions of one- and two-electrode transmitter models. They found that the received voltage and electric field were both enhanced by attaching the ground electrode to the human body [17]. Hwang et al. investigated the effect of the ground electrode on the current distribution through numerical simulation. They found that attaching the ground electrode to the body increased the current from the signal electrode and altered the distribution of electric current in the human body [19]. Fujii et al. numerically and experimentally analyzed the received signal levels using a one-electrode transmitter, a two-electrode transmitter, and a one-electrode receiver. A biological tissue-equivalent solid phantom was used in their experiments. In both the simulations and the experiments, the received signal was larger when the two-electrode transmitter was used [20].

In these studies, the simulation models included only the human arm, and the influence of the torso and the environment surrounding the human body was not considered. In addition, only the strength of the electric field was investigated for the two types of electrode contact conditions. Kazim et al. reported a simulation-based study on the electrode configuration, transmitter/receiver placement on various human body postures, and susceptibility to physiological variations [21]. Although this work provides a comprehensive understanding of HBC, the characteristics of the signal transmission path, including the direction of current flow and capacitive coupling by the electric field, have not been studied in detail. Therefore, the impact of the transmitter electrode contact condition on the signal transmission path and the transmission mechanism has been only partially clarified. Understanding the basic transmission mechanisms of HBC is important for developing design guidelines and applications of HBC.

In this study, the signal transmission paths of one- and two-electrode transmitters were investigated by numerical electromagnetic field analysis. The signal transmission characteristics and impedances in the signal paths were compared. Differences in the signal transmission paths were analyzed by comparing the electric field vector distributions and the electric currents in the human arm. The simulation results were assessed to explain why the received signal is larger when a two-electrode transmitter is used.

The remainder of this paper is organized as follows. Section 2 describes the conditions and geometries of the simulation models of the human body, the two types of the transmitters, and the receiver. Section 3 presents the results of electromagnetic field analysis, and Section 4 discusses the differences between the signal transmission paths under the different contact conditions. Section 5 provides the conclusions reached in this study.

2. Simulation Models of Human Body and HBC Devices

2.1. Simulation Conditions

Signal transmission from a wearable HBC device worn on the wrist to an off-body stationary receiver was selected for analysis in this study. The geometry of the whole model is shown in Figure 1a,b, which shows an enlarged view of the finger touching the receiver electrode.

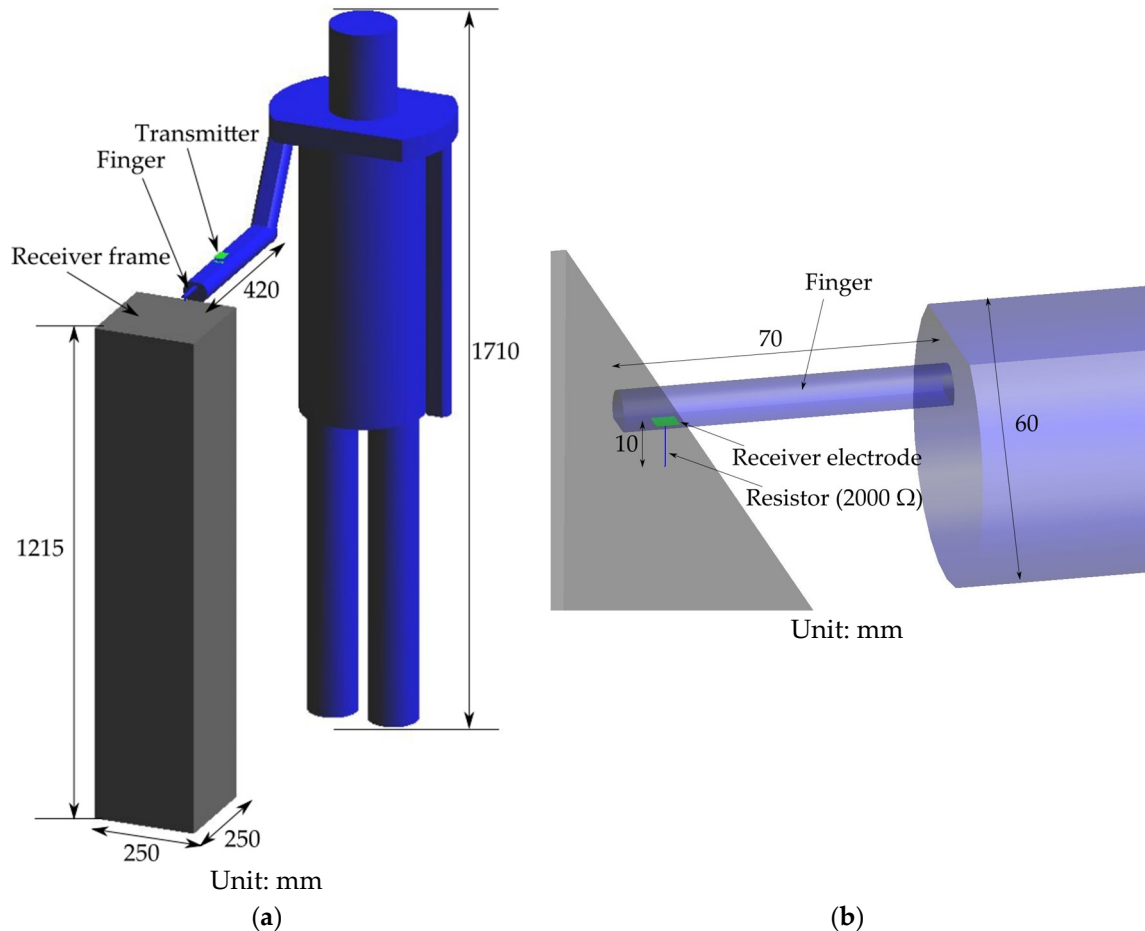


Figure 1. Numerical simulation model. (a) Full model. (b) Detailed view of the finger touching the receiver electrode.

Two types of transmitters, one- and two-electrode transmitters, were separately placed 200 mm from the fingertip as shown in Figure 2. The distributions of the strength and direction of the electric field the transmission characteristics were analyzed using these models.

Simulation software SEMCAD X v14.8.6.1 (SPEAG Software, Zurich, Switzerland) which employs the FDTD method was used for this analysis. Voxel size was 1 mm around the transmitter and the receiver and was gradually increased up to 10 mm with increasing distance from the transmitter and the receiver. Simulation results using coarser voxel size of 2–20 mm and finer voxel size of 0.5–5 mm were evaluated to confirm that the choice of the voxel size was appropriate. Differences in received signal amplitudes and impedances between the transmitter electrodes were less than 3%, and variation in distribution of the electric field was negligible. All the results presented in this paper were obtained using voxel size of 1–10 mm. The simulation space was 1100 mm × 635 mm × 1810 mm, which was determined by setting 50 mm space between the boundary and the human body and the receiver models. Perfectly matched layer of 13 layers was adopted as the boundary condition.

The signal frequency was set to 10 MHz instead of 21 MHz, which was recommended by the IEEE standard, because this frequency has been used in many previous studies. For example, Hachisuka et al. have reported that the transmission characteristic of HBC was maximized at a frequency of 10 MHz [22]. Details of the human body, transmitter, and receiver models will be presented in the following sections.

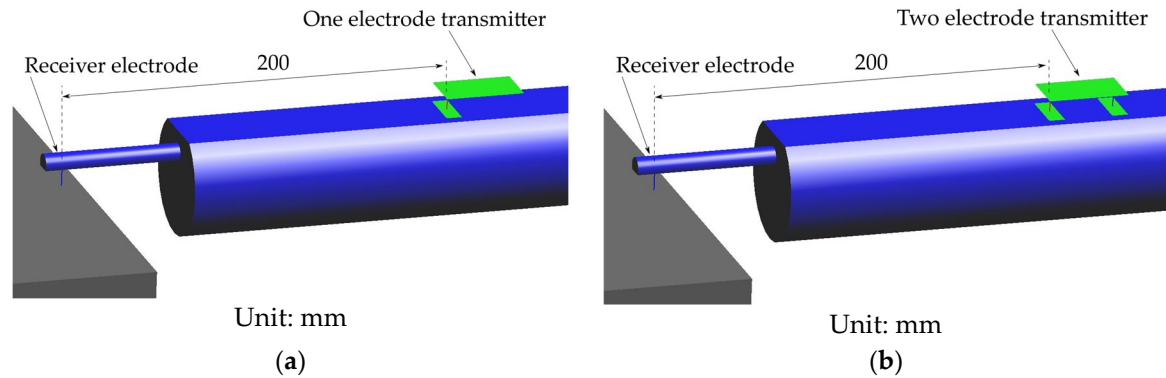


Figure 2. Location of the transmitter and the receiver electrode around the arm: (a) One-electrode transmitter; (b) Two-electrode transmitter.

2.2. Whole Human Body Model

The whole human body model had a height of 1710 mm. The transmitter was placed at the wrist and the off-body receiver was placed in front of the human body as shown in Figure 1a. The floor was not modeled in the present simulation, because the influence of the floor on the transmission is small [12]. The human body model was a homogeneous muscle model with uniform electrical properties. Although the actual human body is composed of various tissues with various electric properties, a qualitative analysis of the transmission characteristics and electric field distribution can be performed using only muscle models. For example, Fujii et al. compared electric field distribution using a realistic high-resolution whole-body model and a homogeneous muscle model at 10 MHz and concluded that the simplified model closely resembled that of the realistic model [20]. Muramatsu et al. used the same realistic model and calculated electric field distribution and impedance between the transmitter electrodes by replacing several body tissues by other tissues and proposed a three-layered model composed of skin, fat, and muscle [23]. Muramatsu further compared this three-layered model with a homogeneous muscle model and concluded that the patterns of electric field distribution were similar, whereas there were some differences in quantitative values [24]. Based on these past findings, it was concluded that the homogeneous muscle model was appropriate for analysis of the signal transmission path. The electric properties of the human body model were equal to that of the muscle at 10 MHz. The relative permittivity ϵ_r was 170, and the electrical conductivity σ was 0.62 S/m [25].

2.3. Transmitter and Receiver Models

A wearable transmitter worn on the human wrist was modeled as shown in Figure 3. The transmitter model consisted of a signal source with an output impedance of 50 Ω , a conductive plate representing a circuit board, electrodes that are in contact with the human body, and conductive wires. The one-electrode transmitter had a signal electrode connected to the signal source, as shown in Figure 3a, and the two-electrode transmitter had a signal electrode and a ground electrode as shown in Figure 3b. The dimensions of the circuit board and electrodes were 40 mm \times 24 mm, and 8 mm \times 24 mm, respectively, and the distance between the electrodes and the board was 10 mm. The circuit board, electrodes, and wires were modeled as perfect electric conductors with no electrical resistance. A sinusoidal signal with an amplitude of 1 V and a frequency of 10 MHz was applied between the transmitter circuit board and the signal electrode.

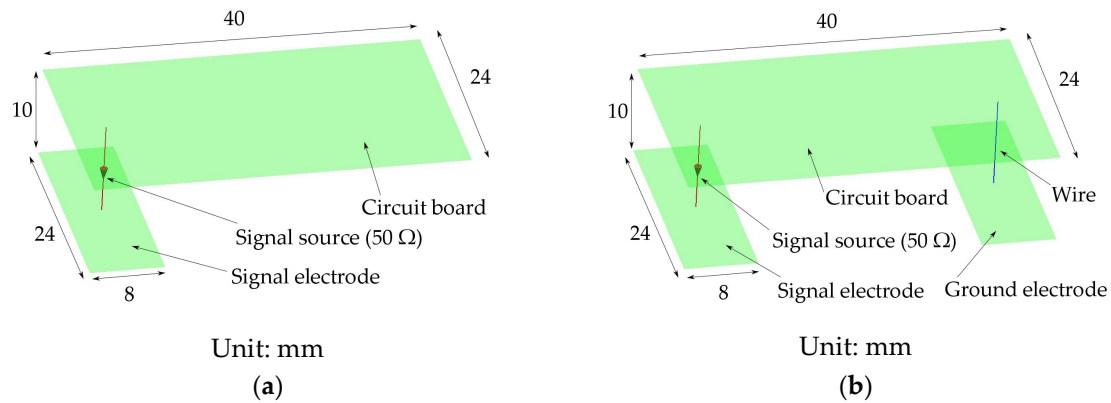


Figure 3. Transmitter models: (a) One-electrode transmitter; (b) Two-electrode transmitter.

The stationary receiver was modeled as shown in Figure 1a,b. The receiver consisted of a frame, a receiver electrode and an input resistor. The dimensions of the receiver electrode were 5 mm × 5 mm. A 2000 Ω resistor was installed between the top of the frame and the electrode, as shown in Figure 1b. The voltage measured across this resistor during signal reception was regarded as the received voltage. The frame of the receiver and the receiving electrode were modeled as perfect electric conductors.

3. Results

3.1. Transmission Characteristics and Impedance between the Transmitter Electrode

Table 1 gives the transmission characteristics of the one- and two-electrode transmitters. The transmission characteristics were evaluated by the ratio between the received signal amplitude and the amplitude of the transmitter output. The transmission characteristic of the two-electrode transmitter was 26 dB greater than that of the one-electrode transmitter.

Table 1. Transmission characteristics and input impedance.

Structure of Transmitter	One-Electrode	Two-Electrode
Transmission characteristics (dB)	−50.4	−24.1
Impedance between transmitter electrodes Z_{in} (Ω)	$33.3 - j69.7 \times 10^2$	$79.9 - j10.8$

Sensitivity of the electric properties in this simulation was evaluated by changing the values by ±12%. The relative permittivity ϵ_r was changed from 170 to 150 and 190, and the electrical conductivity σ was changed from 0.62 S/m to 0.55 S/m and 0.69 S/m. The transmission characteristics ranged from −50.5 dB to −50.0 dB for the one-electrode transmitter and −24.3 dB to −24.0 dB for the two-electrode transmitter. From these results, it was concluded that the sensitivity was sufficiently low for the present simulation.

The impedance Z_{in} between the transmitter electrode and the ground electrode of the transmitter was calculated. In the case of the one-electrode transmitter, the circuit board was used as the ground electrode. The impedance Z_{in} is the total impedance of all external factors viewed from the output terminals of the signal source not including the resistance inside the transmitter. Table 1 gives the calculated values of Z_{in} . The imaginary part of Z_{in} for the one-electrode transmitter was approximately 200 times larger than the real part. This is because the ground is floating in the one-electrode transmitter and the signal path contains capacitive couplings.

In contrast, the imaginary part of the Z_{in} for the two-electrode transmitter was much smaller. This is because there is a direct signal path between the signal and ground electrodes that passes through the human body without capacitive coupling in the air. This result suggests that the electric passing through the human body contributes more to the signal transmission in the two-electrode transmitter than in the one-electrode transmitter. It should be noted, however, that the signal that reaches the receiver is only a small part of the total current that flows out of the transmitter electrode. Therefore, the electric field distribution around the transmitter and the receiver must be investigated to assess the total current.

3.2. Distribution of Electric Field

3.2.1. Electric Field Strength Distribution

The distribution of the electric field around the arm is shown in Figure 4. The plane shown in Figure 4 is a vertical cross-section that passes through the feed point of the transmitter viewed from the right side of the human body model. Figure 4b shows the electric field distribution of the one-electrode transmitter. The electric field is distributed mainly above right arm in this case. In the case of the two-electrode transmitter, a strong electric field of -20 to -10 dB was distributed around the transmitter, inside the arm, and below the arm, as shown in Figure 4c.

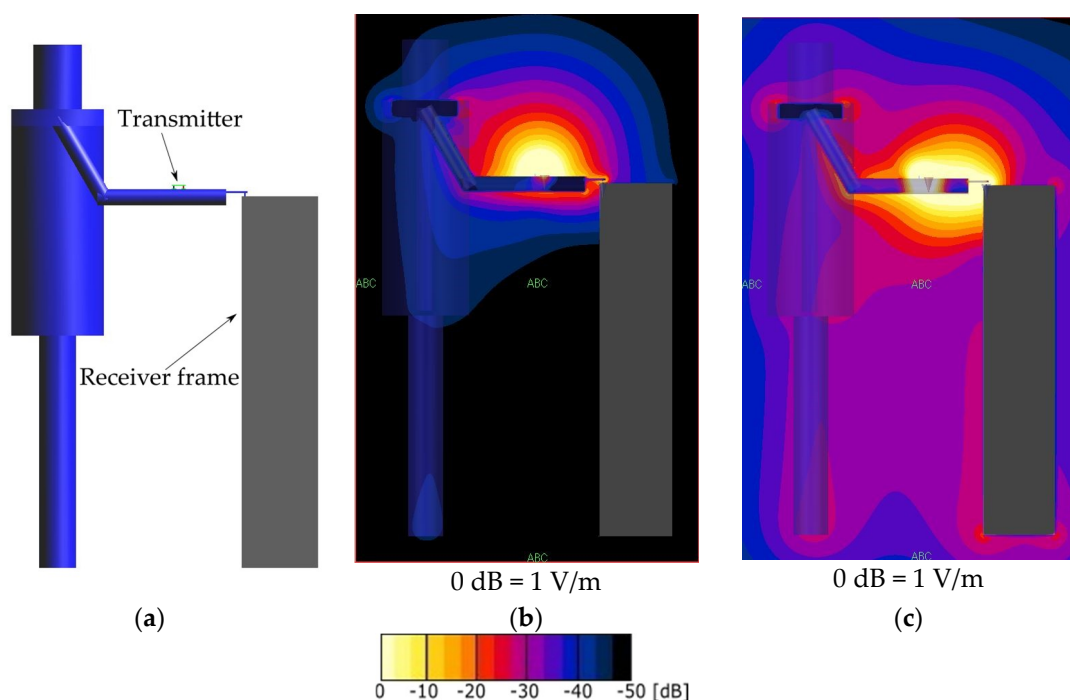


Figure 4. Electric field distribution in a vertical cross-section containing the transmitter, the receiver, and the human arm viewed from right side of the model. (a) Configuration of the simulation model. (b) Electric field distribution for the one-electrode transmitter. (c) Electric field distribution for the two-electrode transmitter.

3.2.2. Electric Field Vector Distribution

Figure 5 shows the vector distribution of the electric field when the one-electrode transmitter was used. The plane shown in Figure 5a,b is a vertical cross-section passing through the feed point of the transmitter as viewed from the right side of the human body model. This distribution was obtained when the maximum received voltage was recorded. The direction of each arrow represents the vector of the electric field at that point, and the color of the arrows and stream lines represents the

strength of the electric field. Figure 5a shows that the electric field in the one-electrode case travels from the surface of the arm through the space around the arm to the circuit board and is distributed symmetrically around the transmitter. Figure 5b shows a wider view of the same distribution as in Figure 5a, including the human body and the receiver. The electric field excited in the human body and under the arm was weaker than that above the arm. The signal path was concentrated locally in the space above the arm because the only return path is through the capacitive coupling of the floating ground.

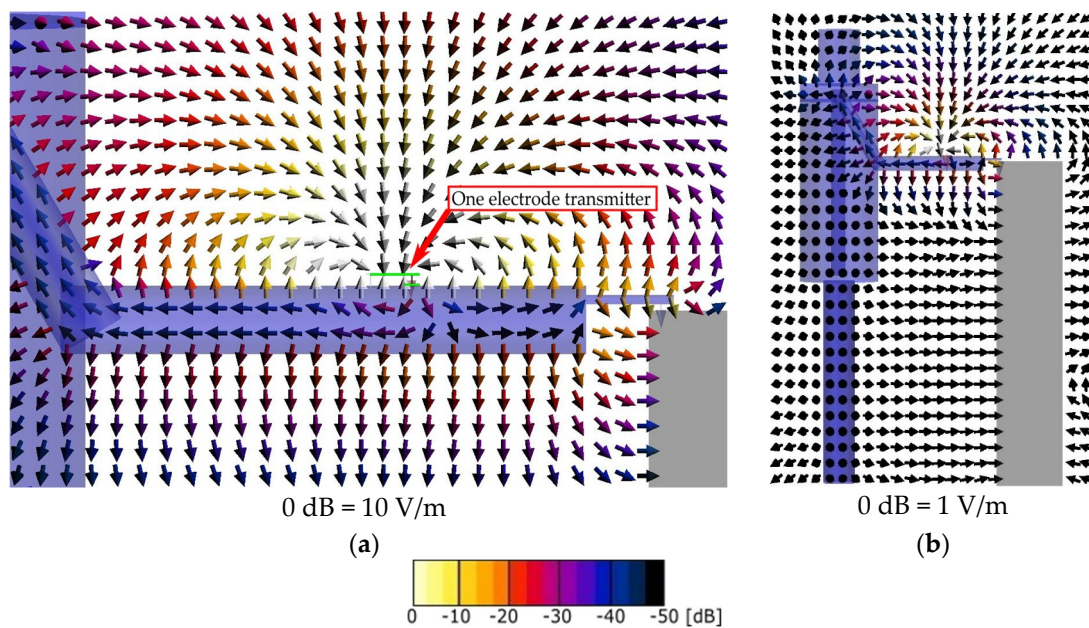


Figure 5. Direction and strength of the electric field in the one-electrode transmitter case. (a) Distribution around the transmitter and the arm. (b) Distribution in a wider area including the whole human body.

Figure 6 shows the vector distribution of the electric field when the two-electrode transmitter was used. A strong electric field was distributed in the space above and below the arm, as shown in Figure 6a. In the space above the arm, the electric field traveled in two directions; coupling occurred from the arm to the circuit board of the transmitter and from the arm to the surface of the receiver frame. In the space below the arm, the electric field from the surface of the arm was directed to the upper arm and the surface of the receiver frame. In the case of the two-electrode transmitter, both the electrical current inside the arm and the capacitive coupling via the air contributed to signal transmission. The distribution in a wider area is shown in Figure 6b. This figure shows that there was a relatively strong electric field distribution between the surface of the receiver frame and the torso. This electric field represents the capacitive coupling between the human body and the receiver frame.

In order to evaluate the influences of realistic objects such as clothes, torso and legs were covered with sheet that had relative permittivity ϵ_r of 3 and electric conductivity σ of 0 S/m, and thickness of 5 to 10 mm. The electric properties are the same as that of polyester. There were no noticeable differences in the direction and strength of the electric field, and the received signal amplitudes.

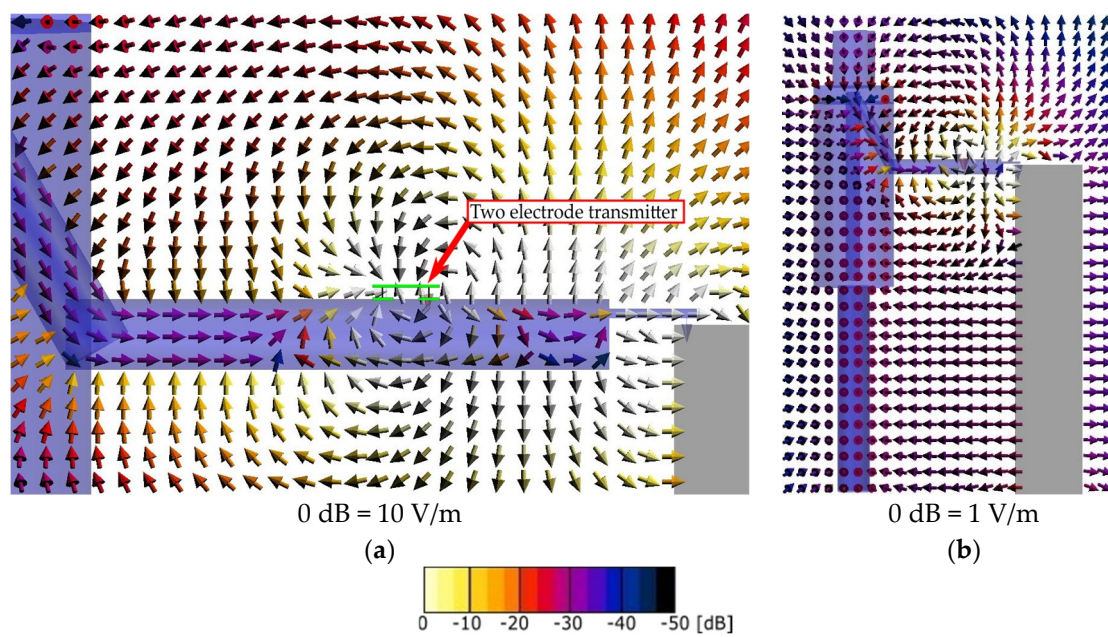


Figure 6. Direction and strength of the electric field in the two-electrode transmitter case. (a) Distribution around the transmitter and the arm. (b) Distribution viewed in a wider area including the whole human body.

3.3. Electric Current in the Arm

The amount of electric current passing through cross-sections along the arm was then evaluated. Figure 7 shows the locations of the analyzed cross-sections. The cross-sections were set at 50 mm intervals from the center of the transmitter circuit board ($X = 0$ mm) with distances toward and away from the body represented by negative and positive X , respectively. The current that flowed in the X -direction and the current I_R that flowed into the receiver resistor were recorded, at the time of the maximum received voltage.

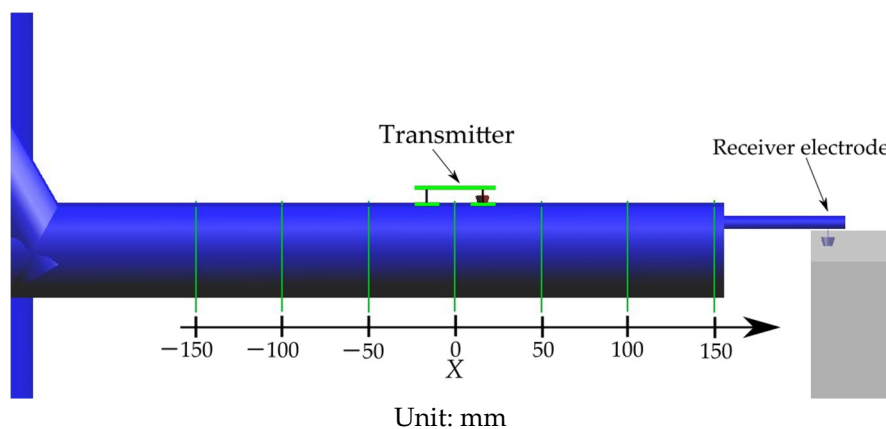


Figure 7. Locations of cross-sections along the arm model.

Table 2 gives the amount of electric current flowing through the arm in the when one- and two-electrode transmitters cases. When the one-electrode transmitter was used, the electric current was positive for positive X negative for negative X . This means that the current on the positive X side of the transmitter flowed from the transmitter to the finger and that on the negative X side flowed in the opposite direction. The magnitude of the current passing through the cross-sections of the arm

decreased as the distance from the transmitter increased. The current that flowed into the resistor of the receiver was 1.50 μA .

Table 2. Current through the cross-sections and the receiver resistor.

X (mm)	−150	−100	−50	0	50	100	150	I_R
Current (One-electrode) (μA)	−11.2	−12.2	−16.1	−59.3	6.63	2.95	1.79	1.50
Current (Two-electrode) (μA)	32.8	32.6	34.6	−7500	34.0	31.3	31.3	31.2

When the two-electrode transmitter was used, the current flowed in the same direction, from the elbow to the finger, for both positive and negative X. A large negative current flowed just beneath the transmitter. This means that a large amount of current flowed directly from the signal electrode to the ground electrode through the human body. The magnitude of the current passing through the cross-sections decreased as the distance from the transmitter increased. The current that flowed into the receiver resistor was 31.2 μA .

3.4. Comparison with Experimentally Measured Values

Received signal was measured experimentally to compare with the simulation results. The transmitter was powered by a small battery (CR2032) and the circuit board and the electrodes had the same dimensions used in the simulation. The frequency was 10 MHz and the output signal amplitude was 744 mV. The receiver consisted of a preamplifier and a battery-powered oscilloscope to measure the output of the preamplifier. The preamplifier and the oscilloscope were placed on a tall box that had the same dimensions as the receiver frame in the simulation. The surface of the box was covered with aluminum foil, which was connected to the ground of the receiver circuit. Although it is often mentioned in the literatures that the measuring apparatuses affected the capacitive coupling in HBC, we assumed that the battery-powered oscilloscope acted as part of the receiver ground and had little effect on the overall signal path in this case. Received signal was measured for five times by a single subject. The results are given in Table 3. The transmission characteristic was evaluated by the ratio between the amplitudes of the received signal and the transmitter output. The difference between the one- and two-electrode transmitters was 18.3 dB for the experiment and 26.3 dB for the simulation. It was concluded that these similarities verified the reliability of the simulation.

Table 3. Received signal amplitude measured by experiment.

	Received Signal Amplitude (mV)	Standard Deviation (mV)	Transmission Characteristic (dB)	
			Experiment	Simulation
One-electrode	6.58	0.26	−41.1	−50.4
Two-electrode	53.9	0.85	−22.8	−24.1

4. Discussion

The above analysis of the electric field strength distribution and current flow revealed the differences between the signal transmission behaviors of the one- and two-electrode transmitters. The results are qualitatively summarized in Figure 8a,b. In the case of the one-electrode transmitter, the electric field spread from the transmitter to the space above the arm and not inside the arm. In the case of the two-electrode transmitter, the electric field was distributed above and below the arm and penetrated the arm. Furthermore, when the two-electrode transmitter was used, the electric field was distributed more intensely between the receiver frame and the torso than when the one-electrode transmitter was used.

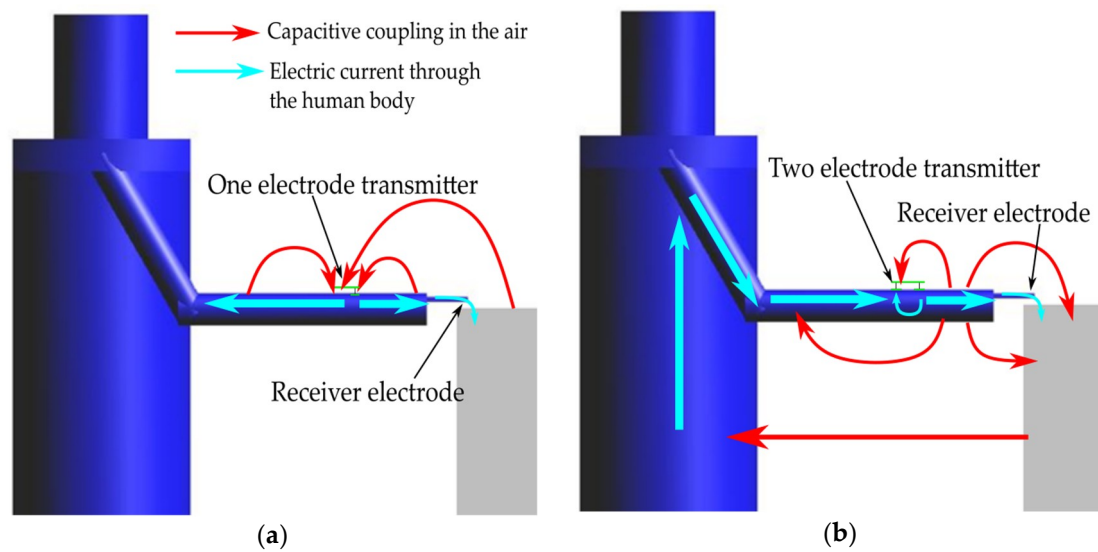


Figure 8. Transmission signal path: (a) Signal path for the one-electrode transmitter. (b) Signal path for the two-electrode transmitter.

Furthermore, in the one- and two-electrode transmitter cases, the current flowed in opposite directions in part of the human forearm between the transmitter and the elbow. This means that the only return path of the one-electrode transmitter is through the capacitive coupling of the floating ground of the transmitter. In contrast, in the case of the two-electrode transmitter, current flowed from the torso, through the upper arm, and to the ground electrode of the transmitter that was in contact with the arm. The capacitive coupling between the receiver ground (i.e., the receiver frame) and the torso and lower parts of the human body allowed the current to flow from the receiver ground to the torso. The capacitive coupling between the receiver ground and the underside of the arm also contributed to the return path. In effect, the area of the ground electrode of the transmitter was enlarged by putting the ground electrode of the transmitter in contact with the human body. It was concluded that this increased coupling is the mechanism producing the larger received signal when the two-electrode transmitter was used.

The signal transmission path and mechanism of HBC revealed in this study are not readily apparent from the distributions of electric field strength that are often reported in previous studies. The method used in this study to analyze the difference between the one- and two-electrode transmitters can be used to analyze other HBC configurations. The results will be useful for the development of HBC applications in terms of device placements and practical choice of electrode configurations.

5. Conclusions

Signal transmission path of human body communication from a wearable transmitter worn on the wrist to an off-body stationary receiver touched by the user's finger was investigated. Numerical simulation results of electric field strength distribution, electric field vector distribution, and electric current in the human body were compared for one-electrode transmitter and two-electrode transmitter. When the signal and ground electrodes of the transmitter were in contact with the human arm, i.e., the two-electrode transmitter, capacitive coupling between the receiver ground and the human torso was much stronger than that of the one-electrode transmitter. As a result, there was electric current flow inside the torso, upper arm, elbow, and to the ground electrode of the transmitter. The increased capacitive coupling and the current flow inside the human body contributed to stronger return path. In the case of one-electrode transmitter, the only return path was through the capacitive coupling of the floating ground. This difference in the transmission path explains why the received signal was larger when two-electrode transmitter was used. Transmission path analysis in this study contributes to the

better understanding of signal transmission mechanism of HBC and will be useful for developing HBC applications.

Author Contributions: Conceptualization, K.Y.; Data curation, K.Y. and Y.N.; Formal analysis, K.Y., Y.N., K.S., D.M. and F.K.; Funding acquisition, K.S.; Investigation, K.Y.; Methodology, K.Y.; Project administration, K.S.; Supervision, K.S.; Writing—Original draft, K.Y.; Writing—Review & editing, Y.N., K.S., D.M. and F.K.

Funding: This research was partly funded by Japan Science and Technology Agency A-STEP Program AS272S001a.

Conflicts of Interest: The authors declare no conflict of interest.

References

- Movassaghi, S.; Abolhasan, M.; Lipman, J.; Smith, D.; Jamalipour, A. Wireless Body Area Networks: A Survey. *IEEE Commun. Surv. Tutor.* **2014**, *16*, 1658–1686. [[CrossRef](#)]
- IEEE Standard for Local and Metropolitan Area Networks, Part 15.6: Wireless Body Area Networks. ISBN 9780738172064. Available online: <https://ieeexplore.ieee.org/document/6161600/> (accessed on 11 June 2018).
- Ghamari, M.; Janko, B.; Sherratt, R.S.; Harwin, W.; Piechockic, R.; Soltanpur, C. A Survey on Wireless Body Area Networks for eHealthcare Systems in Residential Environments. *Sensors* **2016**, *16*, 831. [[CrossRef](#)] [[PubMed](#)]
- Pereira, M.D.; Alvarez-Botero, G.A.; De Sousa, F.R. Characterization and Modeling of the Capacitive HBC Channel. *IEEE Trans. Instrum. Meas.* **2015**, *64*, 2626–2635. [[CrossRef](#)]
- Li, M.; Song, Y.; Li, W.; Wang, G.; Bu, T.; Zhao, Y.; Hao, Q. The modeling and simulation of the galvanic coupling intra-body communication via handshake channel. *Sensors* **2017**, *17*, 863. [[CrossRef](#)] [[PubMed](#)]
- Song, Y.; Zhang, K.; Hao, Q.; Hu, L.; Wang, J.; Shang, F. A finite-element simulation of galvanic coupling intra-body communication based on the whole human body. *Sensors* **2012**, *12*, 13567–13582. [[CrossRef](#)] [[PubMed](#)]
- Baldus, H.; Corroy, S.; Fazzi, A.; Klabunde, K.; Schenk, T. Human-Centric Connectivity Enabled by Body-Coupled Communications. *IEEE Commun. Mag.* **2009**, *47*, 172–178. [[CrossRef](#)]
- Xu, R.; Ng, W.C.; Zhu, H.; Shan, H.; Yuan, J. Equation environment coupling and interference on the electric-field intrabody communication channel. *IEEE Trans. Biomed. Eng.* **2012**, *59*, 2051–2059. [[CrossRef](#)] [[PubMed](#)]
- Zimmerman, T.G. Personal Area Networks: Near-field intrabody communication. *IBM Syst. J.* **1996**, *35*, 609–617. [[CrossRef](#)]
- Zhu, X.Q.; Guo, Y.X.; Wu, W. Investigation and Modeling of Capacitive Human Body Communication. *IEEE Trans. Biomed. Circuits Syst.* **2017**, *11*, 474–482. [[CrossRef](#)] [[PubMed](#)]
- Xu, R.; Zhu, H.; Yuan, J. Electric-field intrabody communication channel modeling with finite-element method. *IEEE Trans. Biomed. Eng.* **2011**, *58*, 705–712. [[CrossRef](#)] [[PubMed](#)]
- Sasaki, K.; Arai, N.; Muramatsu, D.; Koshiji, F. Evaluation of Ground Loop Through the Floor in Human Body Communication. *Int. J. Wirel. Inf. Netw.* **2017**, *24*, 78–90. [[CrossRef](#)]
- Mao, J.; Yang, H.; Zhao, B. An Investigation on Ground Electrodes of Capacitive Coupling Human Body Communication. *IEEE Trans. Biomed. Circuits Syst.* **2017**, *11*, 910–919. [[CrossRef](#)] [[PubMed](#)]
- Park, J.; Garudadri, H.; Mercier, P.P. Channel Modeling of Miniaturized Battery-Powered Capacitive Human Body Communication Systems. *IEEE Trans. Biomed. Eng.* **2017**, *64*, 452–462. [[CrossRef](#)] [[PubMed](#)]
- Fujii, K.; Ito, K.; Tajima, S. A study on the receiving signal level in relation with the location of electrodes for wearable devices using human body as a transmission channel. In Proceedings of the IEEE Antennas and Propagation Society International Symposium, Columbus, OH, USA, 22–27 June 2003; pp. 1071–1074. [[CrossRef](#)]
- Sung, J.B.; Hwang, J.H.; Hyoun, C.H.; Kim, J.K.; Park, D.G.; Kang, S.W. Effects of ground electrode on signal transmission of human body communication using human body as transmission medium. In Proceedings of the 2006 IEEE Antennas and Propagation Society International Symposium, Albuquerque, NM, USA, 9–14 July 2006; pp. 491–494. [[CrossRef](#)]
- Haga, N.; Saito, K.; Takahashi, M.; Ito, K. Equivalent circuit of intrabody communication channels inducing conduction currents inside the human body. *IEEE Trans. Antennas Propag.* **2013**, *61*, 2807–2816. [[CrossRef](#)]

18. Kurosu, M.; Koshiji, F.; Koshiji, K. Electromagnetic field analysis of human body communication between wearable and stationary devices including the earth ground. In Proceedings of the 2014 International Conference on Electronics Packaging (ICEP), Toyama, Japan, 23–25 April 2014; pp. 744–747. [[CrossRef](#)]
19. Hwang, J.H.; Myoung, H.J.; Kang, T.W.; Kim, S.E.; Kim, J.K.; Hyoung, C.H.; Park, H.I.; Lim, I.G.; Kim, J.B.; Kim, K.S.; et al. Reverse Effects of Transmitter’s Location on the Signal Loss of the Human Body Communication. In Proceedings of the 2008 IEEE Antennas Propagation Society International Symposium, San Diego, CA, USA, 5–11 July 2008; Volume 1, pp. 4–7. [[CrossRef](#)]
20. Fujii, K.; Takahashi, M.; Ito, K. Electric field distributions of wearable devices using the human body as a transmission channel. *IEEE Trans. Antennas Propag.* **2007**, *55*, 2080–2087. [[CrossRef](#)]
21. Kazim, M.I.; Kazim, M.I.; Wikner, J.J. An Efficient Full-Wave Electromagnetic Analysis for Capacitive Body-Coupled Communication. *Int. J. Antennas Propag.* **2015**. [[CrossRef](#)]
22. Hachisuka, K.; Takeda, T.; Terauchi, Y.; Sasaki, K.; Hosaka, H.; Itao, K. Intra-body data transmission for the personal area network. *Microsyst. Technol.* **2005**, *11*, 1020–1027. [[CrossRef](#)]
23. Muramatsu, D.; Koshiji, F.; Koshiji, K.; Sasaki, K. Input Impedance Analysis of a Human Body Communication Transmitter Using a Realistic Human Model and a Simplified Layered Model. *Trans. Jpn. Inst. Electron. Packag.* **2013**, *16*, 528–534. [[CrossRef](#)]
24. Muramatsu, D.; Koshiji, F.; Koshiji, K.; Sasaki, K. Homogenous Arm Model in Impedance Analysis of Electrodes for Human Body Communication. In Proceedings of the 2nd IEEE Global Conf. on Consumer Electronics (GCCE 2013), Tokyo, Japan, 1–4 October 2013.
25. FCC Webpage: Radio Frequency Safety—Body Tissue Dielectric Parameters Tool. Available online: <https://www.fcc.gov/general/body-tissue-dielectric-parameters> (accessed on 11 June 2018).



© 2018 by the authors. Licensee MDPI, Basel, Switzerland. This article is an open access article distributed under the terms and conditions of the Creative Commons Attribution (CC BY) license (<http://creativecommons.org/licenses/by/4.0/>).